INL/CON-22-66002-Revision-0

Thermal Model of Oxide Growth for Full Size Fuel Plate Experiments in the Advanced Test Reactor

June 2022

Grant L Hawkes, Hikaru Hiruta

Changing the World's Energy Future

INL is a U.S. Department of Energy National Laboratory operated by Battelle Energy Alliance, LLC

INL/CON-22-66002-Revision-0

Thermal Model of Oxide Growth for Full Size Fuel Plate Experiments in the Advanced Test Reactor

Grant L Hawkes, Hikaru Hiruta

June 2022

Idaho National Laboratory
Idaho Falls, Idaho 83415

http://www.inl.gov

Prepared for the
U.S. Department of Energy
Under DOE Idaho Operations Office
Contract DE-AC07-05ID14517

Thermal Model of Oxide Growth for Full Size Fuel Plate Experiments in the Advanced Test Reactor

Grant Hawkes*, Hikaru Hiruta*

*Idaho National Laboratory, 2525 Fremont, MS 3870, Idaho Falls, Idaho 83415, Grant.Hawkes@inl.gov, Hikaru.Hiruta@inl.gov

INTRODUCTION

The full-size plate number one (FSP-1) irradiation test designed for irradiation testing of plate type fuel is planned to be irradiated in the Advanced Test Reactor (ATR) at the Idaho National Laboratory (INL). This FSP-1 experiment is a non-instrumented drop-in test where aluminum-clad fuel plates are cooled directly by the ATR Primary Coolant System (PCS) water. This experiment is one of a series of experiments being irradiated at ATR for the United States High Performance Research Reactor (USHPRR) program. This fueled experiment contains aluminum-clad fuel full-size plates consisting of monolithic U-10Mo. Previous thermal analyses have been documented concerning oxide growth [1] and thermal safety margins [2] for similar U-10Mo mini plate experiments.

This analysis is part of the thermal safety analysis of the experiment to be irradiated in ATR. Departure from nucleate boiling ratio (DNBR) and flow instability ratio (FIR) have been calculated for the flow coastdown condition-2 and the reactivity insertion accident condition-2 (RIA2) transient. The purpose of this paper is to investigate the thermal margin of the fuel meat during a RIA2 transient when oxide has accumulated on the plate surfaces acting as an insulator.

The FSP-1 experiment has one hardware design and will be irradiated in the Northeast Flux Trap (NEFT) as shown in Figure 1 for four ATR cycles (60 days each) with variable lobe power from cycle to cycle. FSP-1 has three specimen types/condition including full burn (FB), intermediate power (IP), and thick fuel (TF), arranged in distinct fuel-meat axial length segments within swaged frame assemblies. Each frame assembly has a twin, giving a total of six fueled frame assemblies and substituting fueled frame assemblies for dummy frame assemblies when needed as shown in Figure 2. The fuel plate thickness for all three plate types is 0.049 to 0.050-in. The FB, IP, and TM fuel meat thicknesses are 0.085-in., 0.016-in., and 0.025-in. respectively with aluminum 6061 as the cladding material. The fuel meat span for each plate type is 1.5-in., while the fuel meat height for each type of plate is approximately 47.25-in.

This paper discusses a thermal analysis performed on the FSP-1 experiment using a new correlation for calculating oxide growth on the plate surfaces during irradiation. An evaluation was also performed to simulate a RIA2 transient at various stages of oxide growth to investigate if the peak fuel temperature would exceed the minimum fuel blister threshold temperature. The ABAQUS [3] finite element and heat transfer code was used to perform this simulation.

Model Description

The FSP-1 experiment capsule configuration is shown in Figure 3. The ABAQUS model includes 6 fuel plates and two edge rails for each fuel plate, inner and outer baskets, and inner and outer coolant channels along with seven coolant channels next to the fuel plates. The coolant inlet temperature and pressure are 125°F and 372 psia, and the core pressure drop is 77 psid. A flow restrictor with a 1.244-in. square hole orifice will be placed below the end fitting to obtain a desired coolant velocity in the fuel plate coolant channels equal to 14.0 m/s. Coolant flows were obtained from a hydraulic analysis. Water coolant channels are 0.200-in. between fuel plates. Fuel thermal properties come from the U-Mo Handbook in [4]. Aluminum material properties are taken from [5].

A reactor physics analysis using the MCNP neutronics code [7] provides fission power and fission density in the fuel plates. The heating rate was input into ABAQUS using a FORTRAN subroutine. The coordinates of the MCNP grid cells are used in the ABAQUS subroutine to identify the grid cell in which a particular finite element is located, and the heating rate in the element is set to the fission power from the corresponding MCNP grid cell.

Shown in Figure 4 is a cut-away view of the entire finite element mesh. Water convection finite elements are shown in blue. Hexagonal eight-noded brick finite elements are used. Eight finite elements span across the fuel meat with two finite elements through the aluminum cladding on each side for a total of 12 across the fuel plate. The entire model consists of approximately 1.5 million finite elements. The fuel meat zone has 190 elements along its length and 16 across the width. Figure 5 shows the finite element mesh of the fuel plates, edge rails, and inner and outer baskets and ram rod.

The 95% lower bound blister threshold temperature [4] varying with fission density (FD) is defined as:

- For fission density (FD) $\leq 1.5 \times 10^{21}$ fissions/cm^3, Tb (lower 95% prediction bound) = 478°C
- For FD $\geq 1.5 \times 10^{21}$ fissions/cm^3, Tb = (lower 95% prediction bound) = $3.25 \times 10^7 \cdot FD^{-0.2282}$ (°C).

Forced convection heat transfer is modeled with a film temperature-varying heat-transfer coefficient between the flowing water and solid surfaces. The GAPCON subroutine in ABAQUS was used to calculate the heat transfer coefficient between the water and the fuel plates. Water properties are evaluated at the film temperature. The Reynolds number Re_D is calculated in Eq 1 as:

(1)

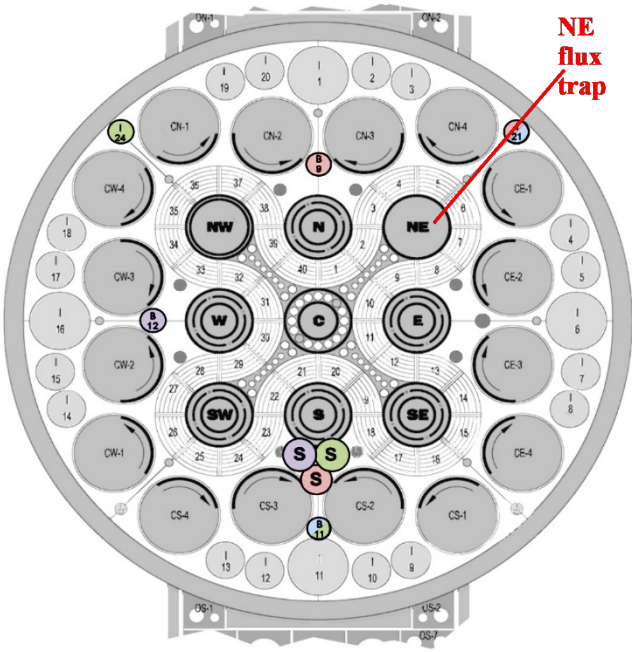

Figure 1. ATR core cross section for the FSP-1 experiment.

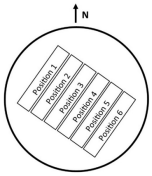

Cycle	1	2	3	4
Lobe (MW)	20	18	18	18
Cycle Length (days)	60	60	60	60
Pos. 1	FB	FB	FB	FB
Pos. 2	IP	IP	Al-DUM	Al-DUM
Pos. 3	Al-DUM	TF	TF	Al-DUM
Pos. 4	Al-DUM	TF	TF	Al-DUM
Pos. 5	IP	IP	Al-DUM	Al-DUM
Pos. 6	FB	FB	FB	FB

Figure 2. Fuel plate loading by geometry and cycle.

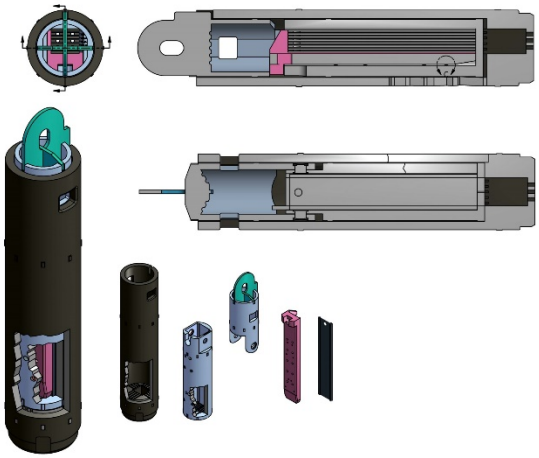

Figure 3. FSP-1 capsule configuration.

Where ρ is the density, v is the velocity, D_H is the hydraulic diameter based on the cross-sectional area and perimeter of the flow channels, and μ is the molecular viscosity. For turbulent internal flow, the friction factor f can be calculated from Eq 2 as:

(2)

The Nusselt number Nu_D using the Gnielinski correlation from Eq 8.63 in Reference [6] was used and is described in Eq 3 as:

(3)

Where Pr is the Prandtl number defined as $\mu c_p/k$ and c_p is the specific heat. The heat transfer coefficient h is then calculated from Eq 4 as:

(4)

Where k is the thermal conductivity. Water properties of density, specific heat, thermal conductivity, viscosity and Prandtl number varying with temperature were input into the GAPCON subroutine.

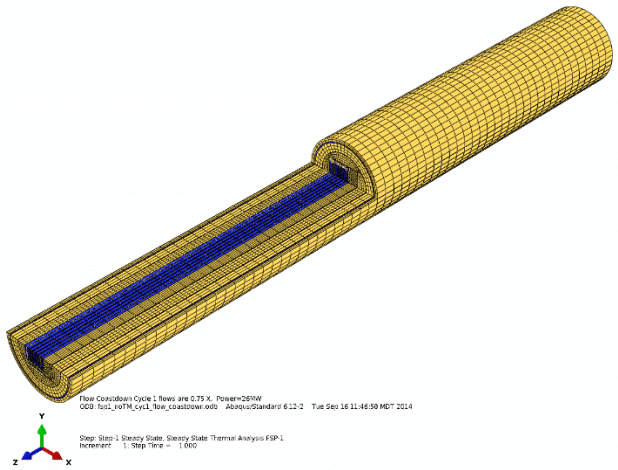

Figure 4. Zoomed in cutaway view of finite element mesh.

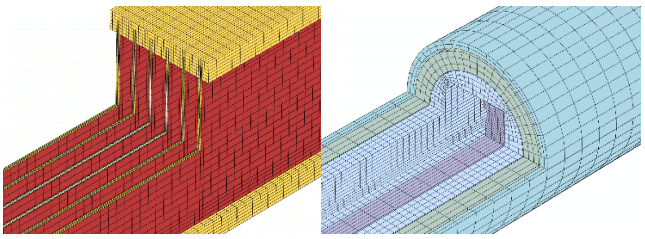

Figure 5. Finite element mesh of fuel plates and aluminum components.

Fission heat rates for the fuel meat and gamma heat rates for the water and aluminum were calculated separately from the MCNP physics and neutronics code and input into ABAQUS. Figure 6 shows the fission heat generation rate (HGR) for the FB plates for all four cycles, IP plates for cycles 1 and 2, and TM plates for cycles 2 and 3.

To account for the oxide layer, the overall heat transfer coefficient applied in the subroutine is calculated in Eq 5 as:

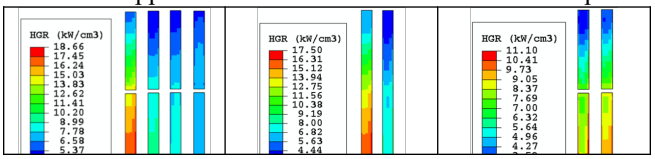

FB	IP	TM

Figure 6. Contour plot of fission heat generation rate (kW/cm^3) for FB plates for all four cycles, IP plates for cycles 1 and 2, and TM plates for cycles 2 and 3.

(5)

where k_{ox} is the thermal conductivity of the oxide (2.25 W/m/K), h_{conv} is described in Eq 4, and the evolution of the oxide thickness varying with time and temperature is described using the 2008 Kim correlation [8]. The oxide growth depends on the surface temperature, pH, water velocity, and heat flux. An initial oxide thickness of 2.0 microns was assumed. A transient simulation of the entire irradiation with 40 hour time steps was simulated. HGRs were linearly interpolated between 100% of the neutronics generated heat rates given at the beginning of each cycle to 90% at the end of each cycle as shown in Figure 7. The drastic change of the IP HGR between the first and second cycle is due to the shadowing of the TM plates being inserted for the 2nd cycle. The peak fission densities of the IP and TM plates were 4.4 and 3.7. The fuel thermal conductivity and blister threshold temperature depend on the fission density.

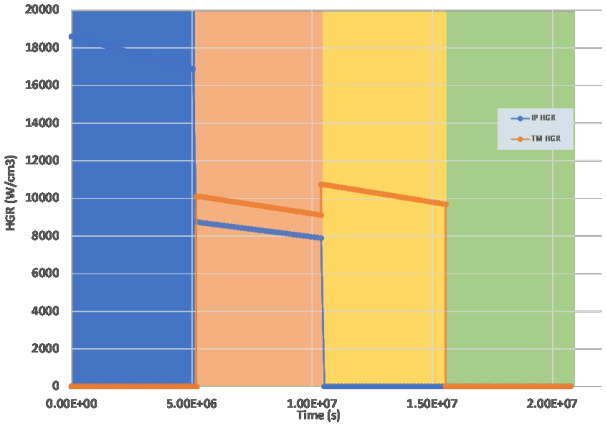

Figure 7. Peak HGR (W/cm^3) for IP and TM plates for four ATR cycles.

RESULTS

The results are shown in Figures 8 through Figure 11. Shown in Figure 8 are contour plots of the oxide thickness for the FB, IP, and TM plates in positions 4-6 respectively. Each plate has its own legend. The TM plates grow to 16.46 microns at the end of cycle 3. Figure 9 shows a history plot of the peak oxide thickness for the IP and TM plates for the 2008 and 2019 Kim [9] oxide correlations. We will use the 2008 Kim correlation as it grows more oxide than the 2019 correlation, but not as much as the ATR modified Griess correlation. Figure 10 shows contour plots of the fuel meat

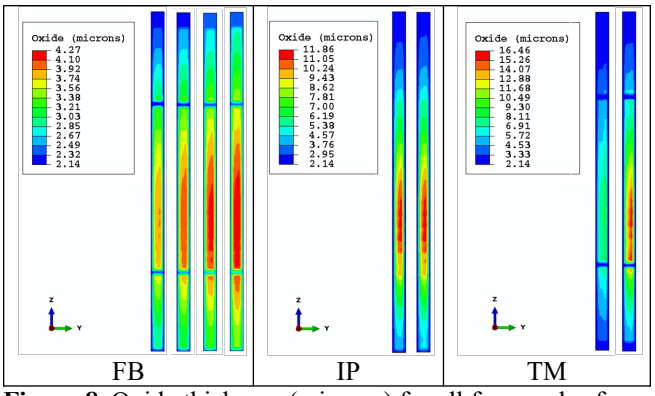

Figure 8. Oxide thickness (microns) for all four cycles for FB plates, cycles 1 and 2 for IP plates, and cycles 2 and 3 for TM plates.

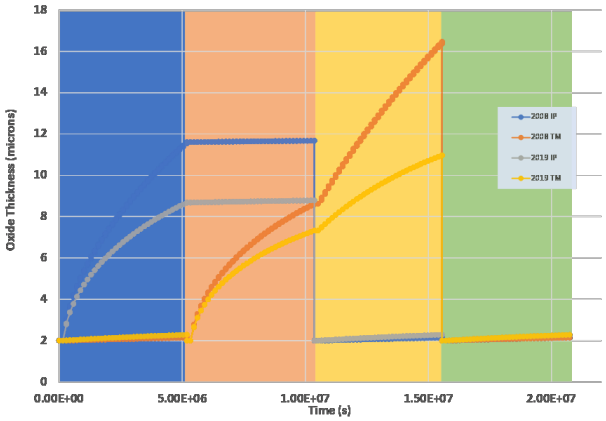

Figure 9. Peak oxide thickness (microns) versus time for IP and TM plates for 2008 and 2019 Kim correlations.

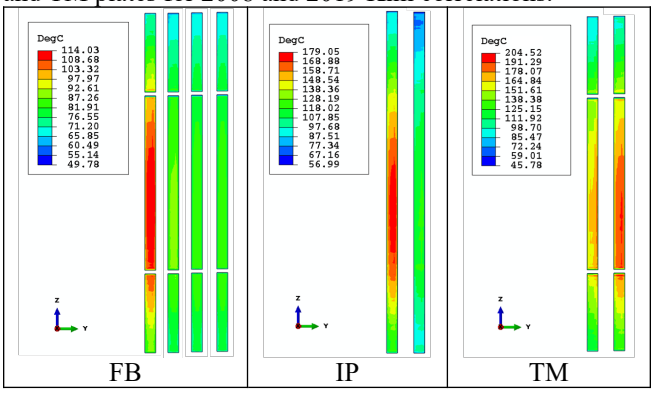

Figure 10. Temperature (°C) contour plots for all four cycles for FB plates, cycles 1 and 2 for IP plates, and cycles 2 and 3 for TM plates.

centerline temperature at the end of each ATR cycle. The thick TM plates have the highest temperature at 204.52°C. Figure 11 shows a temperature history plot of the peak fuel meat temperature for the IP and TM plates. The RIA2 transient has constant flow with a power spike of 83% during 0.16 seconds. Six different RIA2 transients were simulated at the beginning, middle and end of the 2nd and 3rd ATR cycles and plotted in the figure. The blister threshold temperatures for the IP and TM plates are also plotted. The

closest that the peak fuel meat temperature during a RIA2 transient comes to the fuel 95% blister threshold temperature is at the end of the third cycle. It appears that the peak fuel meat temperature at the end of the third cycle during the RIA2 transient rises about 50% of the way to the blister threshold temperature.

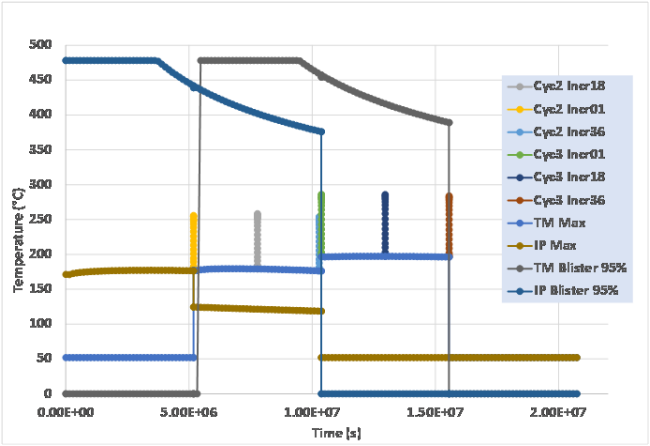

Figure 11. Temperature (°C) history of peak fuel meat during oxide growth and RIA2 transients.

NOMENCLATURE

D	diameter	(m)
f	friction factor	()
h	heat transfer coefficient	(W/m^2/K)
k	thermal conductivity	(W/m/K)
Nu	Nusselt number	( )
Pr	Prandtl number	( )
Re	Reynolds number	( )
Ra	Rayleigh Number	( )
t	thickness of oxide	(m)
T	temperature	(K)
v	velocity	(m/s)

Subscripts

conv convection
D diameter
H hydraulic
tot total
ox oxide

Greek

ρ density (kg/m^3)
μ viscosity (kg/m-s)

CONCLUSIONS

This paper shows results of a simulation of oxide growth using the 2008 and 2019 Kim correlations for the FSP-1 experiment in the ATR. Heat transfer coefficients varying with water temperature were implemented. Oxide growth was calculated in the ABAQUS subroutine GAPCON and had the effect of decreasing the convective heat transfer coefficient. Six different RIA2 transients were simulated during the irradiation of the experiment to discover when the peak fuel meat temperature reached the closest to the 95% blister threshold temperature. This occurred at the end of the third cycle. This peak fuel meat temperature rose to approximately 50% of the way from the steady state temperature to the blister threshold temperature.

ACKNOWLEDGMENTS

Work supported by the U.S. Department of Energy, USHPRR Program, Idaho Operations Office Contract DE-AC07-05ID14517. This research made use of the resources of the High Performance Computing Center at Idaho National Laboratory, which is supported by the Office of Nuclear Energy of the U.S. Department of Energy and the Nuclear Science User Facilities under the same contract number.

REFERENCES

[1] G. L. HAWKES, D. O. CHOE, "Thermal Model of Oxide Growth in Mini Plate Experiments in the Advanced Test Reactor," *ANS Annual Meeting*, Minneapolis, Minnesota, June 9–13, 2019.

[2] G. L. HAWKES, "Thermal Safety Margin Calculation of the MP-2 Experiment in the Advanced Test Reactor," paper number ICONE28-POWER2020-16592, INL/CON-20-57467, ASME ICONE28-POWER2020 Conference, Anaheim, California, August 3–6, 2020.

[3] ABAQUS Standard, Version 6.14-2, SIMULIA, Inc., Providence, Rhode Island, 2015.

[4] B. RABIN, et. al. "Preliminary Report on U-Mo Monolithic Fuel for Research Reactors", INL/EXT-17-40975, Rev. 4, April 2020.

[5] Polkinghorne, S. T. and Lacy, J. M., "Thermophysical and Mechanical Properties of ATR Core Materials," INL Document No. PG-T-91-031, August 1991.

[6] F. INCROPRERA, D. DEWITT, "Fundamentals of Heat and Mass Transfer," 5th ed., John Wiley & Sons, New York, 2002.

[7] The MCNP Code Development Team, "MCNP Code Manual," https://mcnp.lanl.gov/references.shtml, Los Alamos National Laboratory. Accessed Dec. 2017.

[8] Y. S. Kim, et. al., "Oxidation of Aluminum Alloy Cladding for Research and Test Reactor Fuel," doi:10.1016/j.jnucmat.2008.06.032.

[9] Y. S. Kim, et. al., "Aluminum Cladding Oxide Growth Prediction for High Flux Research Reactors," https://doi.org/10.1016/j.jnucmat.2019.151926